Electronic Supplementary Material (ESI) for Physical Chemistry Chemical Physics.

Supplementary Information: "Bishop's hat silicene: a planar square silicon bilayer decorated with adatoms"

Pedro Borlido and Silvana Botti

Institut für Festkörpertheorie und -optik, Friedrich-Schiller-Universität Jena and European Theoretical Spectroscopy Facility, Max-Wien-Platz 1, 07743 Jena, Germany

Miguel A. L. Marques

Institut für Physik, Martin-Luther-Universität Halle-Wittenberg, D-06099 Halle, Germany

S1. DENSITY-FUNCTIONAL TIGHT-BINDING CALCULATIONS

In this section we give more information on the calculations performed using density-functional tight binding[3].

TABLE SI. Summary of the lattice parameters of the structures computed with density-functional tight binding (a and b in Å; γ in degrees).

	a	b	γ
Si-A	5.825	5.825	126.21
Si-B	5.762	5.762	125.12
Si-C	5.224	5.224	90.00
Si-D	5.148	5.247	90.00
Si-E	5.777	5.777	125.84
Si-F	5.168	5.168	90.00

TABLE SII. Supercell size used for the calculations of phonons using density-funcitonal tight binding. Better convergence is achieved by performing the calculations using a rectangular cell. In case of a non-rectangular primitive cell, the phonons bands are then folded back to the primitive Brillouin zone. These cases are indicated with an asterisk and the indicated supercell sizes refer to the conventional supercell.

	Supercell
Si-A	$10 \times 10 \times 1^*$
Si-B	$10 \times 10 \times 1^*$
Si-C	$10 \times 10 \times 1$
Si-D	$10 \times 10 \times 1$
Si-E	$10 \times 10 \times 1^*$
Si-F	$10 \times 10 \times 1$

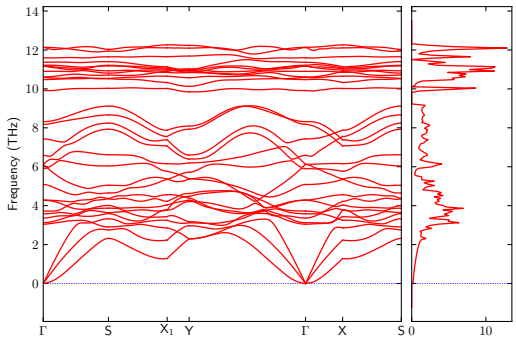

(a) Si-A

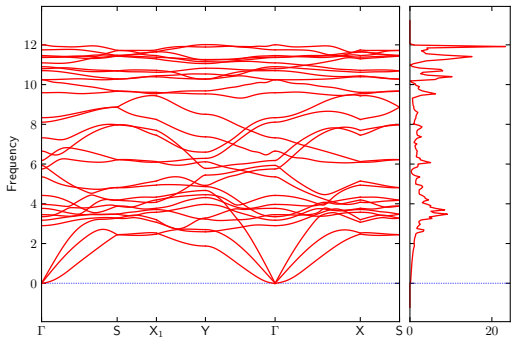

(b) Si-B

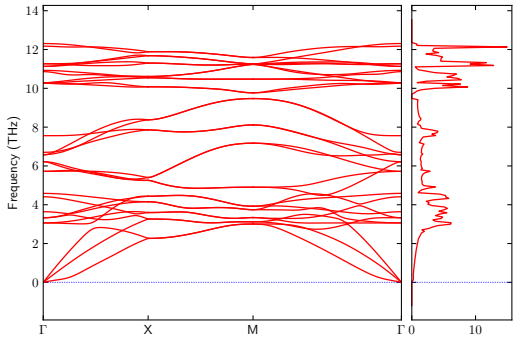

(c) Si-C

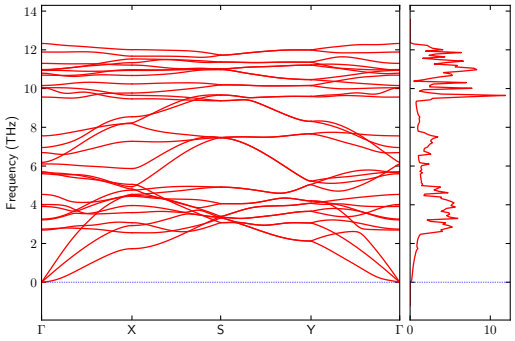

(d) Si-D

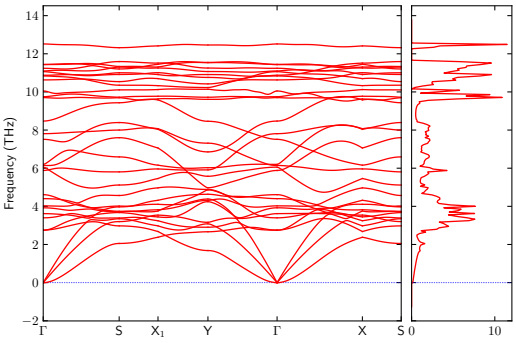

(e) Si-E

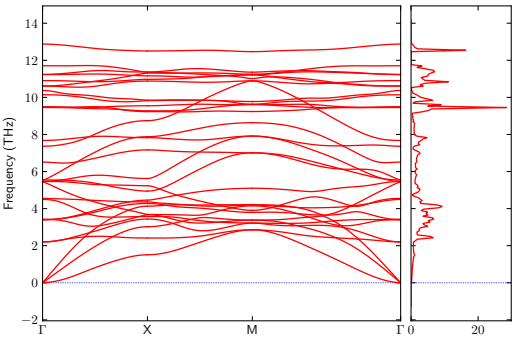

(f) Si-F

FIG. S1. Phonon band structures for the structures discussed in the main text. The calculations are performed using density-functional tight binding.

S2. ELASTIC CONSTANTS

Here we provide more details regarding the calculation of elastic constants. We resort to Voigt's notation 4 for the indices ($1 \to xx$, $2 \to yy$, $3 \to zz$, $4 \to yz$, $5 \to xz$, $6 \to xy$), and for strain tensors ($\boldsymbol{\varepsilon} = (\varepsilon_1, \varepsilon_2, 2\varepsilon_6) = (\varepsilon_{xx}, \varepsilon_{yy}, 2\varepsilon_{xy})$) and stress tensors ($\boldsymbol{\sigma} = (\sigma_1, \sigma_2, \sigma_6) = (\sigma_{xx}, \sigma_{yy}, \sigma_{xy})$). The structures described in the main text belong to the $\frac{2}{m}\frac{2}{m}\frac{2}{m}$, $\frac{2}{m}$ and $\frac{4}{m}\frac{2}{m}\frac{2}{m}$ point groups. Following Ref.[2] we can write the elastic tensor ($\mathbf{C}$) for the bishop-hat two-dimensional structures as

$$\mathbf{C}_{4/m2/m2/m} = \begin{pmatrix} C_{11} & C_{12} & 0 \\ C_{12} & C_{11} & 0 \\ 0 & 0 & C_{66} \end{pmatrix}, \tag{1}$$

and

$$\mathbf{C}_{2/m2/m2/m} = \mathbf{C}_{2/m} = \begin{pmatrix} C_{11} & C_{12} & 0 \\ C_{12} & C_{22} & 0 \\ 0 & 0 & C_{66} \end{pmatrix}. \tag{2}$$

As a consequence, Equations (3), (4), (5) and (6) of Reference [1] can be directly used. The energy densities (up to second order in $\boldsymbol{\varepsilon}$) are then given by

$$\mathcal{U}_{2/m} = \frac{1}{2}C_{11}\varepsilon_{xx}^2 + \frac{1}{2}C_{22}\varepsilon_{yy}^2 + C_{12}\varepsilon_{xx}\varepsilon_{yy} + 2C_{66}\varepsilon_{xy}^2 . \tag{3}$$

where, by setting $C_{11} = C_{22}$, we recover the expression for the more symmetric structures. All elastic constants are uniquely determined using 4 types of strain-modes: uniaxial along x $\left(\begin{smallmatrix} \varepsilon & 0 \\ 0 & 0 \end{smallmatrix}\right)$, uniaxial along y $\left(\begin{smallmatrix} 0 & 0 \\ 0 & \varepsilon \end{smallmatrix}\right)$, hydrostatic $\left(\begin{smallmatrix} \varepsilon & 0 \\ 0 & \varepsilon \end{smallmatrix}\right)$, and shear strain $\left(\begin{smallmatrix} 0 & \varepsilon \\ \varepsilon & 0 \end{smallmatrix}\right)$. The total energies as a function of the strain for each of these modes and each bishop-hat structure are plotted in Figure S2. The angle dependent in-plane Young moduli ($Y_{\mathbf{n}}^{\mathrm{2D}}$ in N/m) and Poisson ratios ($\nu_{\mathbf{n}}$) are shown in Figure S3.

TABLE SIII. Strain modes used for the structures under study.

x-uniaxial	$\left(\begin{smallmatrix}\varepsilon & 0\\ 0 & 0\end{smallmatrix}\right)$	$\mathcal{U}_{2/m} = \frac{1}{2}C_{11}\varepsilon^2$
y-uniaxial	$\left(\begin{smallmatrix}0 & 0\\ 0 & \varepsilon\end{smallmatrix}\right)$	$\mathcal{U}_{2/m} = \frac{1}{2}C_{22}\varepsilon^2$
hydrostatic	$\left(\begin{smallmatrix}\varepsilon & 0\\ 0 & \varepsilon\end{smallmatrix}\right)$	$\mathcal{U}_{2/m} = \frac{1}{2}(C_{11}+C_{22}+2C_{12})\varepsilon^2$
shear	$\left(\begin{smallmatrix}0 & \varepsilon\\ \varepsilon & 0\end{smallmatrix}\right)$	$\mathcal{U}_{2/m} = 2C_{66}\varepsilon^2$

	$Y_{\max}$	$Y_{\min}$	$\nu_{\max}$	$\nu_{\min}$
Si-A	122 (0.0)	85 (46.4)	0.37 (315.8)	0.12 (90.0)
Si-B	141 (90.0)	84 (136.0)	0.40 (45.7)	0.04 (0.0)
Si-C	126 (0.0)	85 (225.0)	0.37 (225.0)	0.07 (0.0)
Si-D	143 (0.0)	85 (226.0)	0.37 (135.6)	-0.01 (0.0)
Si-E	119 (0.0)	74 (55.1)	0.32 (319.6)	0.11 (90.0)
Si-F	116 (0.0)	87 (225.0)	0.32 (225.0)	0.09 (0.0)

TABLE SIV. Values for the maximum and minimum of the Young modulus (in N/m) and Poisson ratio for each of the structures under study. In parenthesis is indicated the direction (in degrees, with respect to the x axis) for the corresponding maxium/minimum. Note that due to the symmetry of the structures, this direction might not be unique.

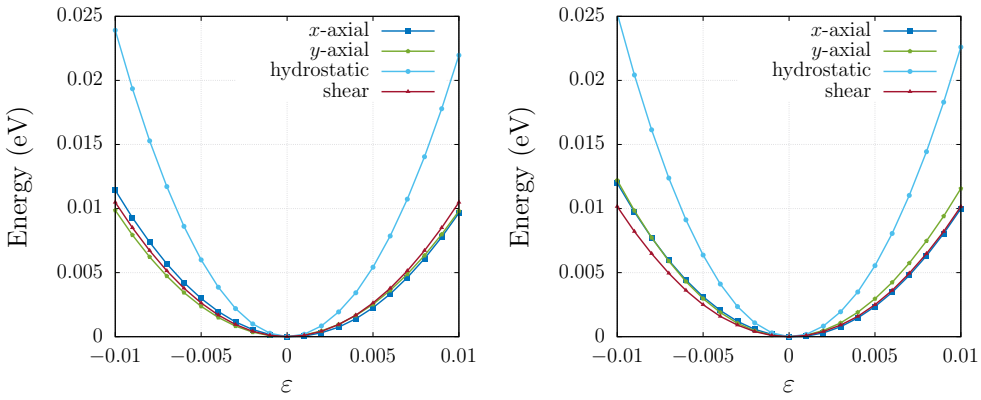

(a) Si-A

(b) Si-B

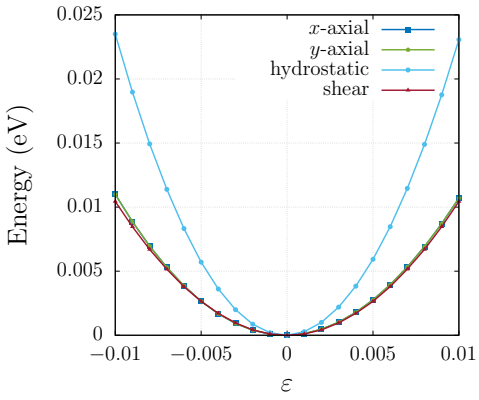

(c) Si-C

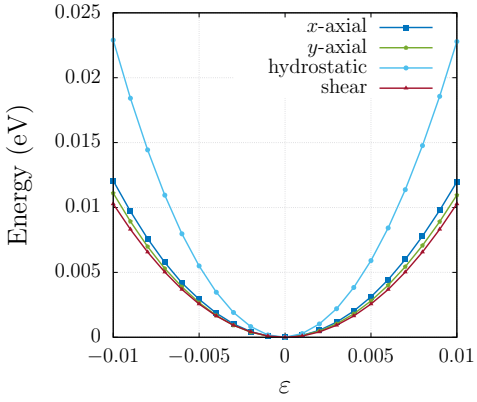

(d) Si-D

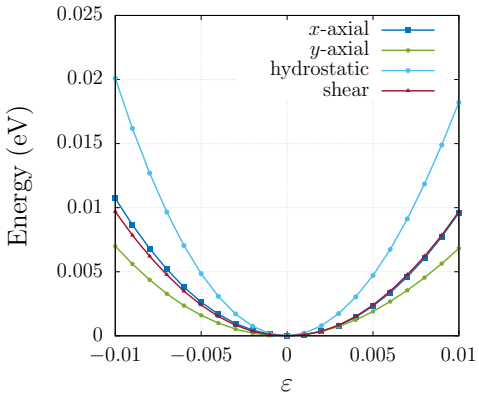

(e) Si-E

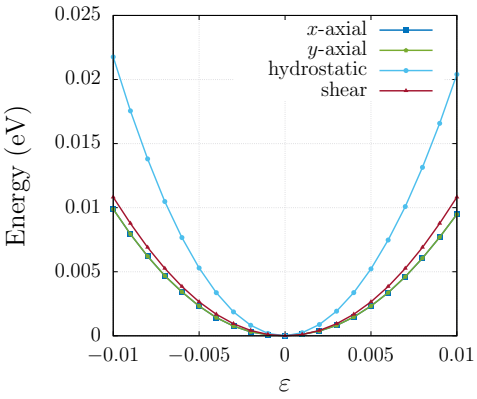

(f) Si-F

FIG. S2. Energy vs. strain curves for the six structures described in the main text. Each curve represents a different strain mode. The origin of the scale was set to the energy of the corresponding optimized structure.

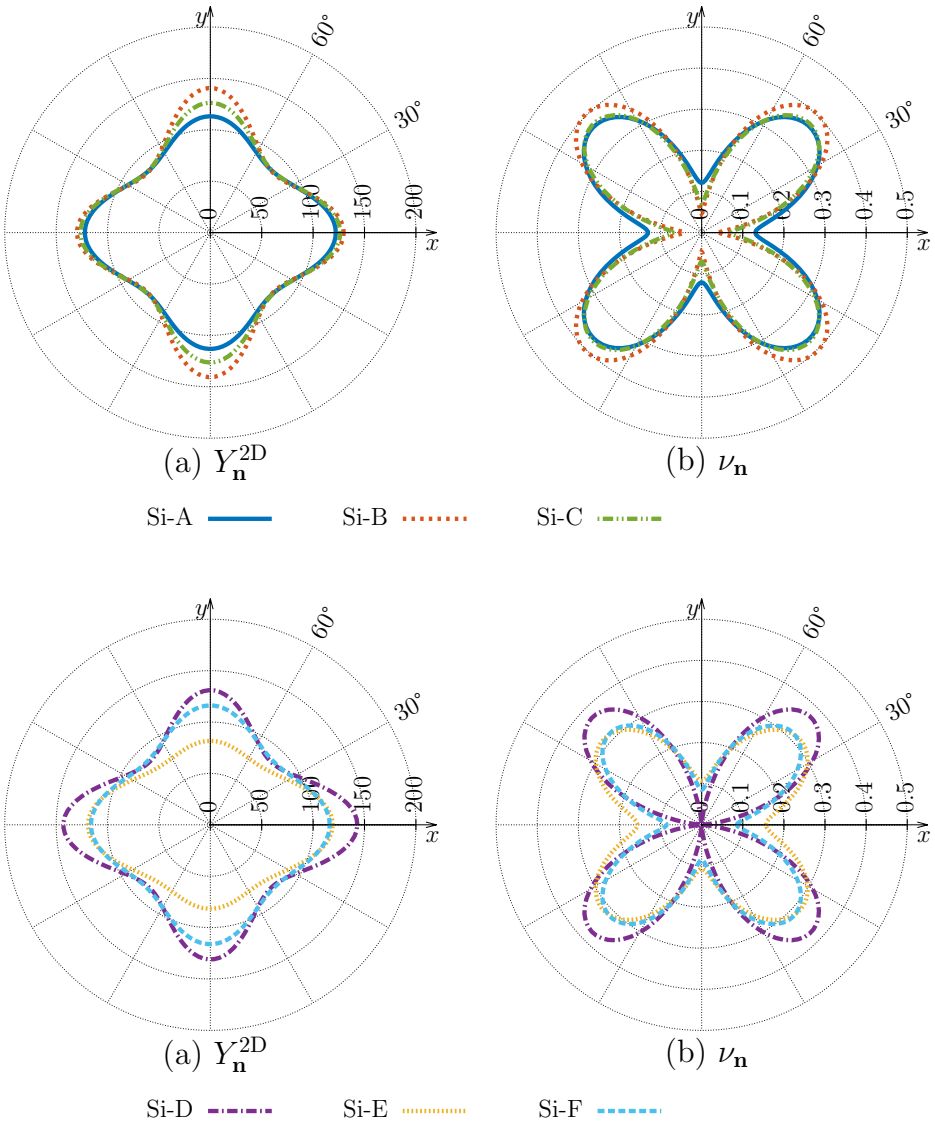

FIG. S3. Absolute values of the direction dependent Young modulus ($Y_{\mathbf{n}}^{2D}$ in N/m) and Poisson ratio ($\nu_{\mathbf{n}}$) for the six structures under study. Cartesian directions are consistent with the axis presented in the main text.

S3. WORK FUNCTIONS

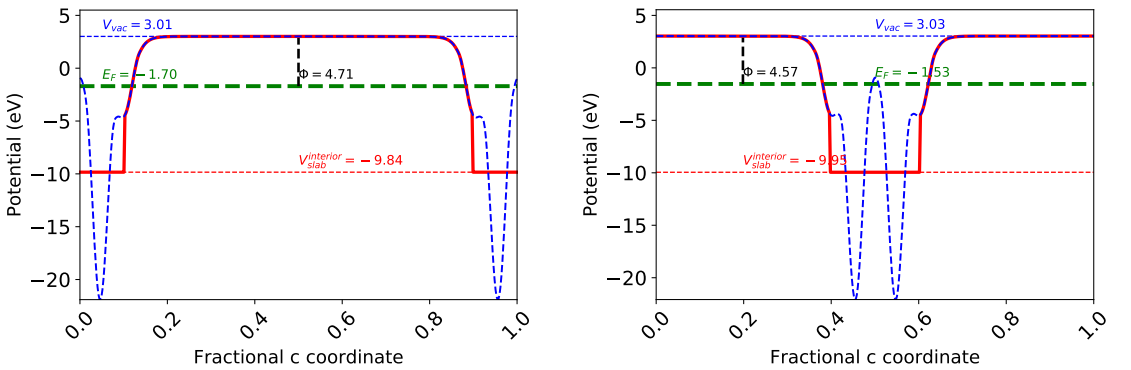

(a) Si-A

(b) Si-B

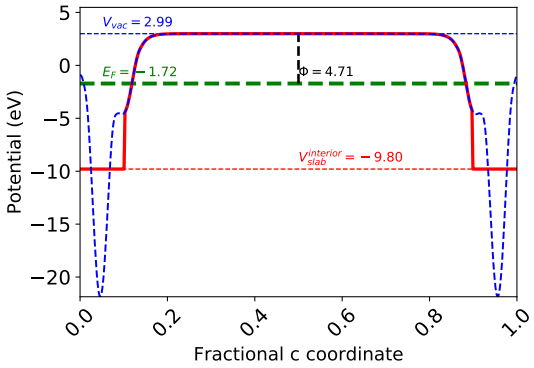

(c) Si-C

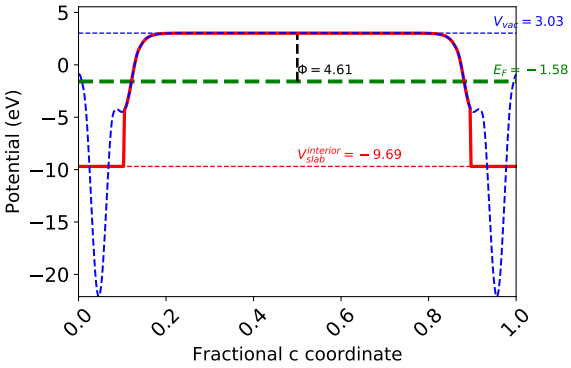

(d) Si-D

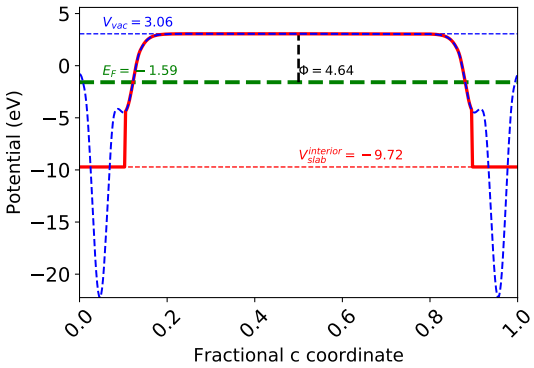

(e) Si-E

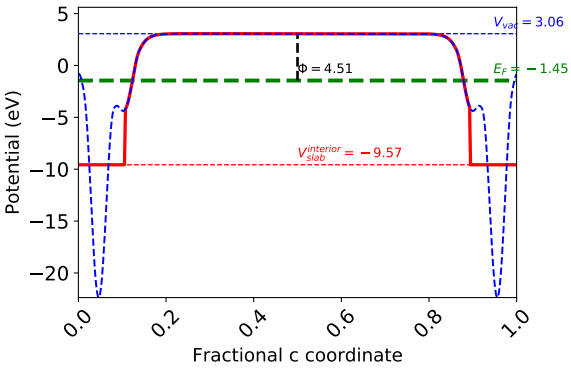

(f) Si-F

FIG. S4. Local electrostatic potentials of the six structures along the direction perpendicular to the layers.

S4. FERMI SURFACES

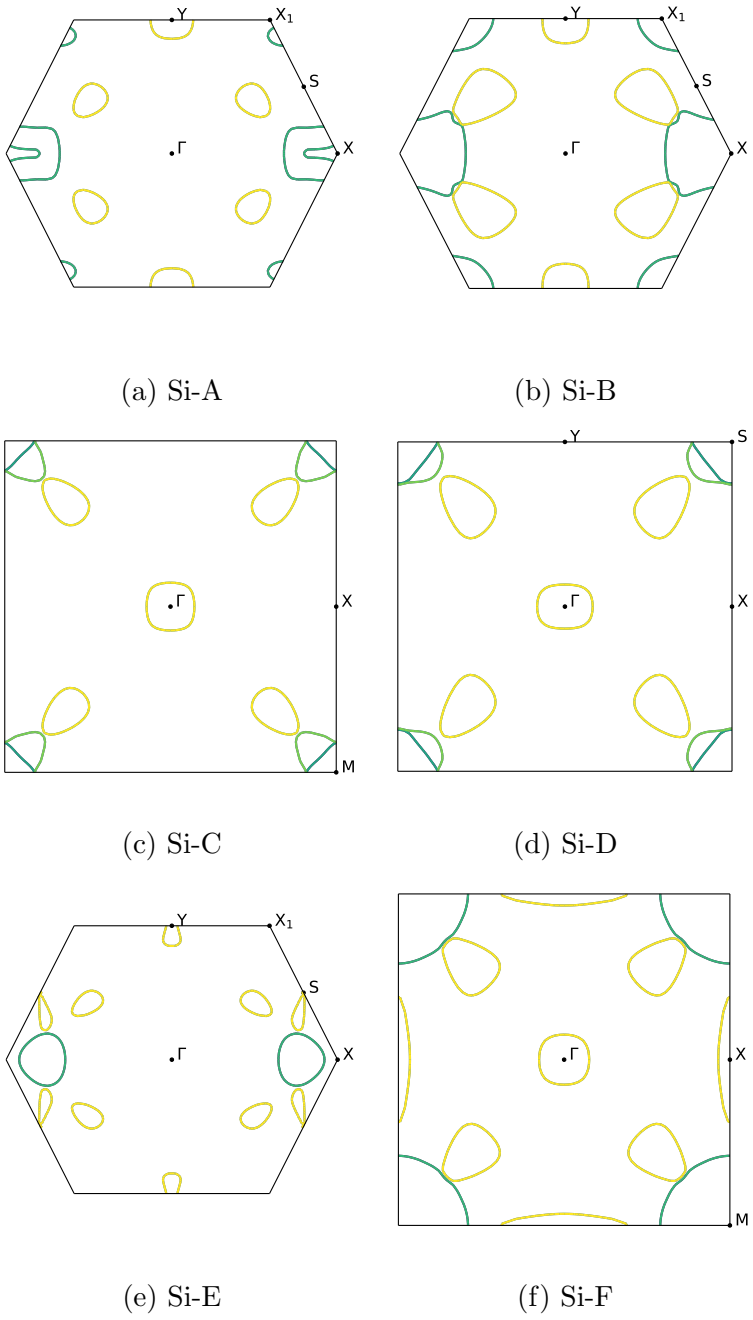

(a) Si-A (b) Si-B

(c) Si-C (d) Si-D

(e) Si-E (f) Si-F

FIG. S5. Fermi surfaces of the six structures.

S5. BANDS WITH SPIN-ORBIT COUPLING

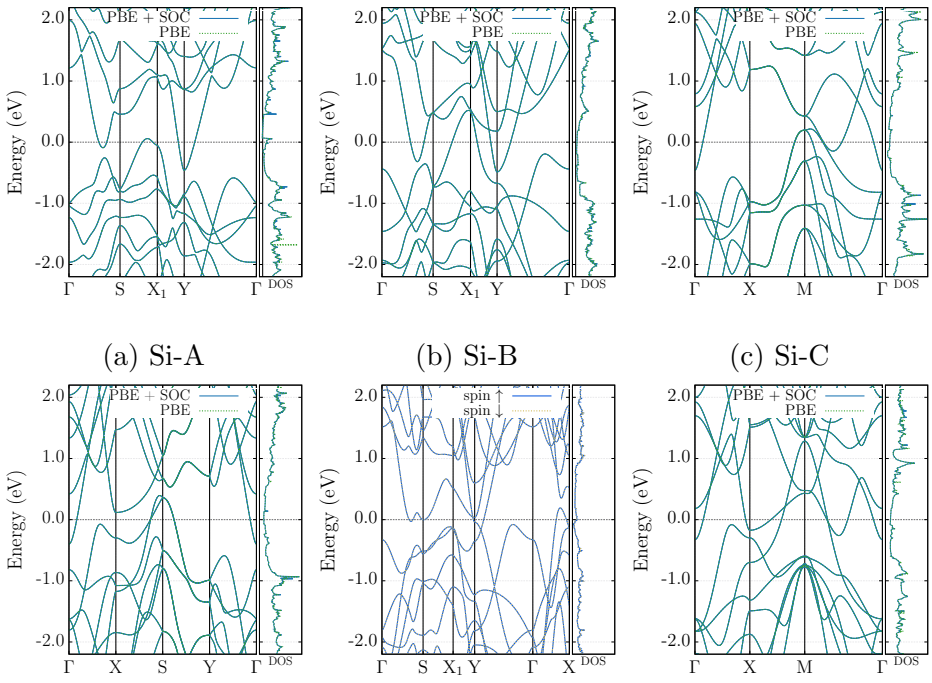

(a) Si-A (b) Si-B (c) Si-C

(d) Si-D (e) Si-E (f) Si-F

FIG. S6. Electronic band structures for the structures under study, computed with PBE and PBE including spin-orbit coupling.

S6. SIMPLE CUBIC SILICON PHONONS

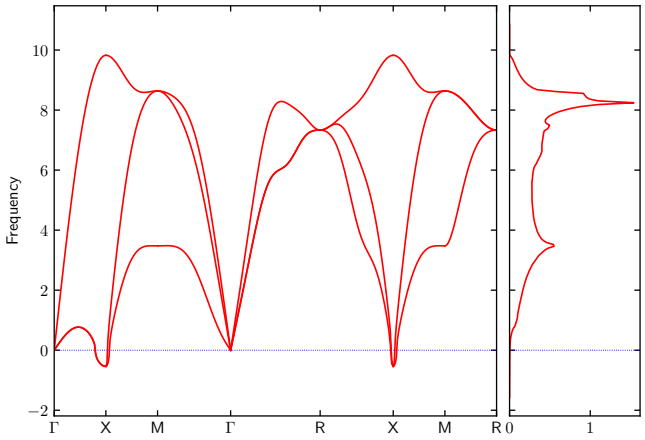

FIG. S7. Phonon band structure for the simple cubic bulk silicon. Frequencies in THz.

S7. MOLECULAR DYNAMICS

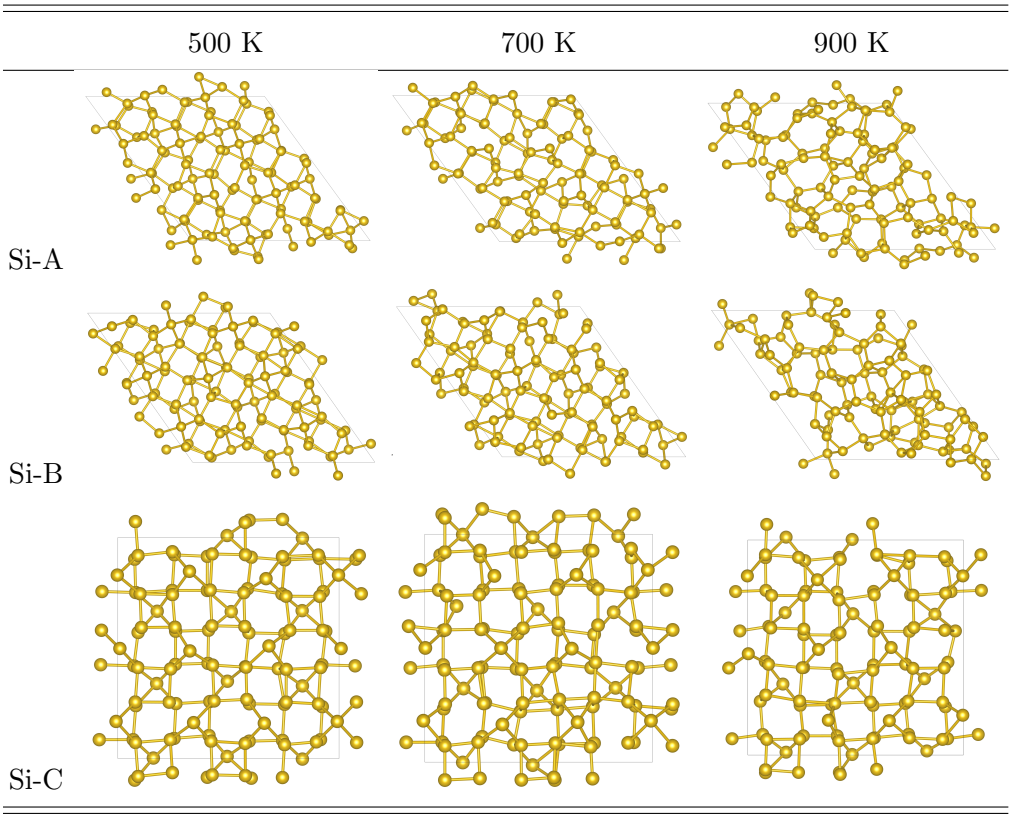

FIG. S8. Structures after molecular dynamics at temperatures of 500 K, 700 K and 900 K.

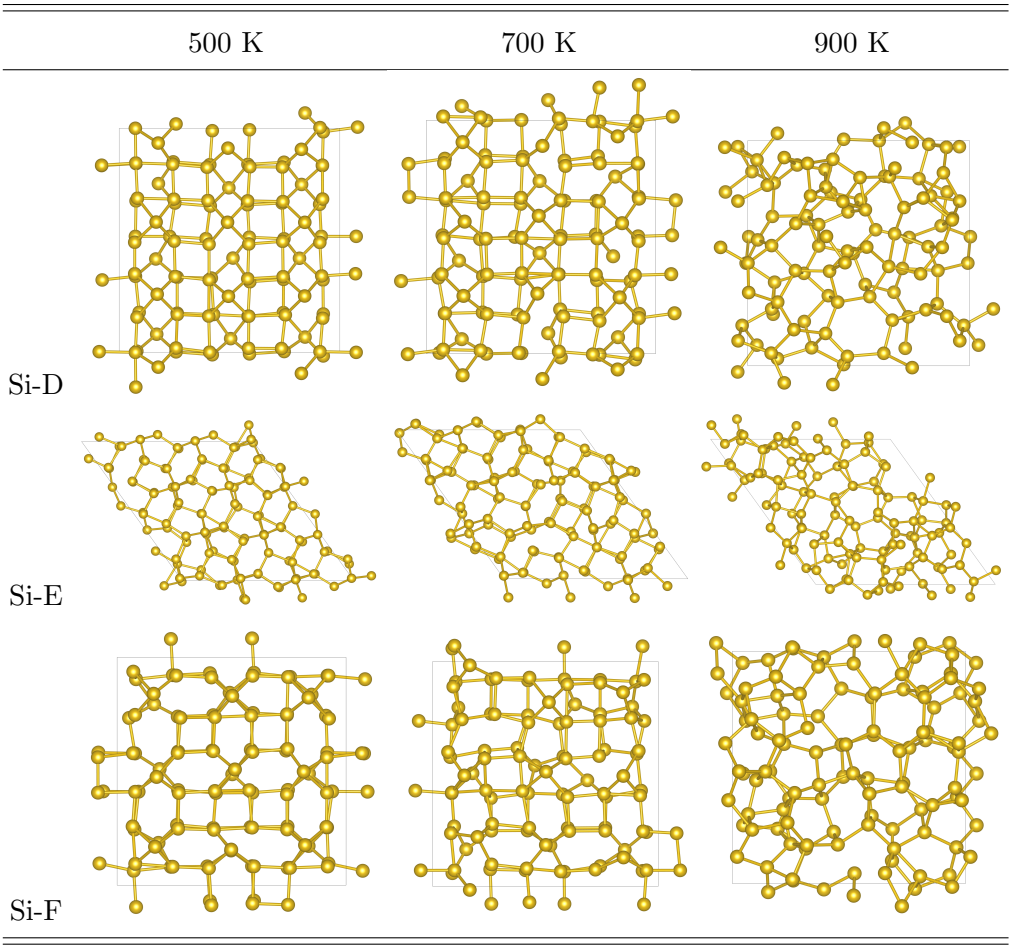

FIG. S8. (cont.) Structures after molecular dynamics at temperatures of 500 K, 700 K and 900 K.

S8. SI-A MULTILAYERS

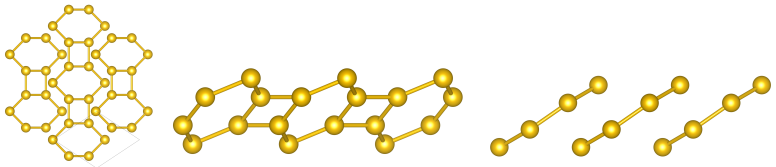

FIG. S9. Crystal structure of the optimized Si-A monolayer, as viewed from the [001] (a), [010] (b) and [110] (c) directions.

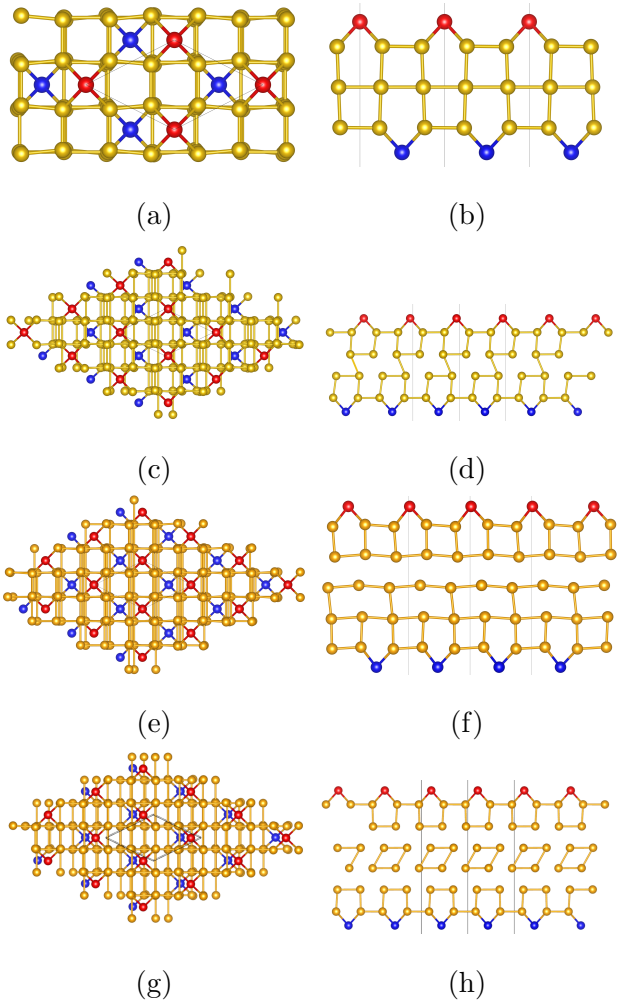

FIG. S10. Crystal structure of the optimized Si-A tri-, tetra-, penta and hexa-layers as viewed from the [001] (left) and [110] (right) directions.

S9. SUBSTRATE COMPATIBILITY

Material	Face	MCIA (Å^2)
ZrO_2 (mp-2858)	[001]	54.54
SiC (mp-11714)	[110]	54.54
$YAlO_3$ (mp-3792)	[001]	54.54
Al (mp-134)	[11$\bar{1}$]	81.81

TABLE SV. Substrates with the smallest minimal coincident interface area (MCIA) for Si-A.

Material	Face	MCIA (Å^2)
$LiNbO_3$ (mp-3731)	[001]	27.03
$LiNbO_3$ (mp-3731)	[100]	27.03
AlN (mp-661)	[111]	27.03
ZrO_2 (mp-2858)	[001]	54.06

TABLE SVI. Substrates with the smallest minimal coincident interface area (MCIA) for Si-B.

Material	Face	MCIA (Å^2)
ZrO_2 (mp-2858)	[001]	27.28
$LiAlO_2$ (mp-3247)	[001]	27.28
YVO_4 (mp-19133)	[11$\bar{1}$]	54.57
Ni (mp-23)	[110]	54.57

TABLE SVII. Substrates with the smallest minimal coincident interface area (MCIA) for Si-C.

[1] E. Cadelano, P. L. Palla, S. Giordano, and L. Colombo. Elastic properties of hydrogenated graphene. *Phys. Rev. B*, 82(23):235414, Dec. 2010.

[2] H. Huntington. The Elastic Constants of Crystals. In *Solid State Physics*, volume 7, pages 213–351. Elsevier, 1958.

Material	Face	MCIA (Å^2)
$LiAlO_2$ (mp-3247)	[001]	26.96
ZrO_2 (mp-2858)	[001]	26.96
ZrO_2 (mp-2858)	[010]	53.92
C (mp-66)	$[10\bar{1}]$	53.92

TABLE SVIII. Substrates with the smallest minimal coincident interface area (MCIA) for Si-D.

Material	Face	MCIA (Å^2)
$LiAlO_2$ (mp-3247)	[001]	53.66
SiC (mp-11714)	[110]	53.66
ZrO_2 (mp-2858)	[001]	53.66
$CdWO_4$ (mp-19387)	[110]	80.49

TABLE SIX. Substrates with the smallest minimal coincident interface area (MCIA) for Si-E.

[3] A. W. Huran, C. Steigemann, T. Frauenheim, B. Aradi, and M. A. L. Marques. Efficient Automatized Density-Functional Tight-Binding Parametrizations: Application to Group IV Elements. *J. Chem. Theory Comput.*, 14(6):2947–2954, June 2018.

[4] W. Voigt. *Lehrbuch der Kristallphysik*. Vieweg+Teubner Verlag, Wiesbaden, 1966.

Material	Face	MCIA ($Å^2$)
ZrO_2 (mp-2858)	[001]	26.62
$LiAlO_2$ (mp-3247)	[001]	26.62
Cu (mp-30)	[110]	26.62
$YAlO_3$ (mp-3792)	[001]	53.23

TABLE SX. Substrates with the smallest minimal coincident interface area (MCIA) for Si-F.